Modulation of Deep-Red to Near-Infrared Room Temperature Charge-Transfer Phosphorescence of crystalline "Pyrene-Box" Cages by coupled ion/guest structural self-assembly

Weixu Feng, Dong Chen, Yan Zhao, Bin Mu, Hongxia Yan, Mihail Barboiu

Modulation of Deep-Red to Near-Infrared Room Temperature Charge-Transfer Phosphorescence of crystalline "Pyrene-Box" Cages by coupled ion/guest structural self-assembly

Weixu Feng,[*,†] Dong Chen,[†] Yan Zhao,[†] Bin Mu,[†] Hongxia Yan[*,†] and Mihail Barboiu[*,‡]

[†]Xi'an Key Laboratory of Hybrid Luminescent Materials and Photonic Device, School of Chemistry and Chemical engineering, Northwestern Polytechnical University, Xi'an 710129, Shaanxi, China.

[‡]Institut Europeen des Membranes, Adaptive Supramolecular Nano-systems Group, University of Montpellier, ENSCM-CNRS, Place E. Bataillon CC047, Montpellier, F-34095, France.

ABSTRACT: Organic cocrystals obtained from multicomponent self-assembly have garnered considerable attention due to their distinct phosphorescence properties and broad applications. Yet, there have been limited reports on cocrystal systems that showcase efficient deep-red to near-infrared (NIR) charge transfer (CT) phosphorescence. Furthermore, effective strategies to modulate the emission pathways of both fluorescence and phosphorescence remain underexplored. In this work, we dedicated our work to four distinct self-assembled cocrystals "Pyrene Box" cages using 1,3,6,8-pyrenetetrasulfonate anions (**PTS**$^{4-}$), 4-Iodoaniline (**1**), Guanidinium (**G**$^{+}$), Diamino-guanidinium (**A$_2$G**$^{+}$), and hydrated **K**$^{+}$ counter cations. The binding of such cations to **PTS**$^{4-}$ platforms adaptively modulating their supramolecular stacking self-assembly with guest molecules **1**, allowing to steer the fluorescence and phosphorescence pathways. Notably, the confinement of guest molecule **1** within "Pyrene Box" **PTSK{1}** and **PTSG{1}** cages, leads to an efficient deep-red to NIR CT phosphorescence emission. The addition of fuming gases like triethylamine and HCl that allows a reversible pH modulations of guest binding, which in turn induce a reversible transition of the "pyrene box" cage between fluorescence and phosphorescence states. This capability was further illustrated through a proof-of-concept demonstration in shrimp freshness detection. Our findings not only lay a foundation for future supramolecular designs leveraging weak intermolecular host-guest interactions to engineer excited states in interacting chromophores, but also broaden the prospective applications of room temperature phosphorescence materials in food safety detection.

INTRODUCTION

Organic room-temperature phosphorescent (RTP) materials have gained remarkable attention due to their vast potential as optoelectronic,[1] anti-counterfeiting label,[2-4] sensing[5, 6] and bioimaging devices.[7, 8] To date, considerable endeavors have been undertaken to craft highly efficient RTP materials. Yet, despite advancements in the field, most available materials predominantly emit colors from cyan to orange,[9-14] with those producing deep-red to NIR emissions being conspicuously limited. The development of RTP materials with NIR emission inherently requires the lowering of the lowest triplet (T1) energy level. This, however, poses dual challenges. Firstly, a diminished T1 level widens the energy gap (Δ_{EST}) between the singlet excited state (S1) and the T1 state, consequently hindering the intersystem crossing (ISC) process. Secondly, a lowered T1 heightens the probability of non-radiative exciton decay, which can drastically curtail phosphorescence lifetime and brightness. As such, formulating an effective and versatile approach to devise organic luminophores exhibiting potent NIR phosphorescence remains a daunting task.

Recently, several organic cocrystals that are crystalline single phase supramolecular solids of self-assembled molecular components have risen in the field due to their captivating phosphorescence properties and a myriad of applications.[15-21] When juxtaposed with other methods aiming to achieve NIR RTP emission, such as single-component crystallization,[22, 23] MOFs,[24] or host-guest doped strategies,[25-27] cocrystals stand out with distinct benefits. Specifically, they eliminate the need for complicate synthesis and enable modulation of the molecular excited state by tweaking the stacking arrangements of different molecular constituents.[28] Currently, one predominant strategy to induce RTP in cocrystals hinges on merging polycyclic aromatic hydrocarbons (PAHs) with halogenated guests. That avoid the excessive aggregation and simultaneously serve as heavy-atom perturbers, thereby amplifying the ISC process of PAHs and significantly boosting their phosphorescence emission.[29, 30] Recent studies have underscored that by fine-tuning molecular stacking patterns, leveraging fluorescence resonance energy transfer (FRET) amid various components, one can effectively harness high-efficiency deep-red to NIR RTP emission in the cocrystal system.[31, 32] However, such design paradigms often necessitate meticulous control over the energy differentials between molecular components. Furthermore, orchestrating and governing the orientation, interplay, and stacking of molecules within a co-crystal matrix remain intricate endeavors. These multifaceted challenges often complicate the pursuit of meticulous designs and the mastery over molecular excited states.[33] Hence, it is crucial to develop simple systems and universal methods to construct efficient and controllable NIR phosphorescent materials to meet the constantly growing practical demands.

We have previously developed a cocrystal supramolecular "Pyrene box" cage, self-assembled from readily accessible 1,3,6,8-pyrenetetrasulfonate anions (**PTS**$^{4-}$) and cations (Guanidinium **G**$^{+}$ or **K**$^{+}$).[34-37] This self-organized capsule is formed by two **PTS**$^{4-}$ platforms laterally capped by H-bonding guanidinium or hydrated **K**$^{+}$ cations. Not only does these host cage systems adhere to the principles of green chemistry, being non-toxic, water-soluble, and environmentally friendly, but also adaptively accommodates guest molecules with a controllable orientation. Given that pyrene derivatives with high conjugation may exhibit a reduced T1 level,[38] integrating the "Pyrene box" with halogenated guest mole-

cules is expected to allow for nuanced control over molecular excited states,

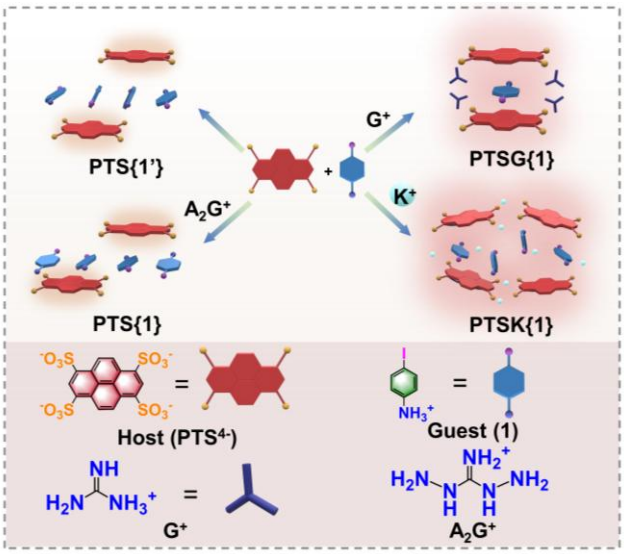

Figure 1. Supramolecular crystalline host "Pyrene box" cages self-assembled from the 1,3,6,8-pyrenetetrasulfonate $\mathbf{PTS^{4-}}$ anions and $\mathbf{A_2G^+}$, $\mathbf{G^+}$, and $\mathbf{K^+}$ cations for adaptive binding of p-iodoaniline (**1**) guest molecules.

yielding efficient, pure RTP spanning longer wavelengths. Additionally, ionic behaviours inherent to these matrixes might induce charge transfer transition features,[39-41] facilitating an even deeper red shift of the emission into the NIR region. Particularly, the encapsulation inherent to the "pyrene box" could also potentially expanded to the cocrystal with controllable stimulus-responsive phosphorescence properties.

With these considerations in mind, we herein introduce a novel concept for the design of NIR RTP cocrystal materials. Four unique cocrystalline systems were synthesized and characterized, with $\mathbf{PTS^{4-}}$ serving as the host molecule and 4-Iodoaniline (**1**) acting as the guest entity. During the crystallization process, we integrated distinct cations ($\mathbf{A_2G^+}$, $\mathbf{G^+}$, and $\mathbf{K^+}$) to adaptively tailor the guest encapsulation, granting meticulous manipulation over the cocrystal system's excited states. Notably, incorporating $\mathbf{G^+}$ and $\mathbf{K^+}$ cations triggered the assembly of the "Pyrene box" in assorted dimensions. Such configurations, in turn, led to the confinement of molecule **1** within the "Pyrene box", enhancing intramolecular charge transfer and ISC processes, yielding a pure deep-red to NIR RTP emission. Our approach of utilizing different cations to construct ternary cocrystal systems resulted in the meticulous regulation of the stacking patterns between the host and guest molecules. This unprecedently explored strategy afforded us the ability to control both the fluores-cence and phosphores-cence emission pathways of $\mathbf{PTS^{4-}}$, alongside fine-tuning its emission wavelength towards the NIR spectrum. Furthermore, these cocrystal materials, constructed under precise supramolecular control, demonstrated a remarkable and distinct fluorescence reactivity to pH-responsive organic amine gases, which underscores their applicability as sensitive sensors for assessing shrimp freshness.

RESULTS AND DISCUSSION

^{1}H NMR Study. The cocrystals **PTS{1'}**, **PTS{1}**, **PTSG{1}**, and **PTSK{1}** were readily synthesized by allowing an acidic aqueous solution containing $\mathbf{PTS^{4-}}$ and protonated 4-Iodoaniline (**1**) to evaporate gradually in the presence of various cations (Figure 1). To ascertain their compositions, we performed ^{1}H NMR analysis. The integration areas suggested that the molar ratios of host to guest molecules are 1:4 for **PTS{1'}** and **PTS{1}**, and 1:1 for **PTSG{1}** and **PTSK{1}** (Figures S1-S6, Table S1). These ratios are supported by subsequent single-crystal structure characterizations. Additionally, the ^{1}H NMR results indicated the presence of ion-pairing interactions between the protonated cationic **1** and $\mathbf{PTS^{4-}}$ anions. This was evident from the noticeable upfield and downfield shifts in the benzene proton peaks of **1** when compared to spectra recorded without the "Pyrene box" (Figure S7). The minor variations in proton signals between **PTS{1}** and **PTS{1'}** may stem from differences in their sample concentrations. Importantly, the pronounced upfield shifts of the protons of **1** in the presence of $\mathbf{G^+}$ further imply the formation of "Pyrene box" cages in the aqueous solution.

Crystal Structure. We subsequently undertook a comprehensive analysis of various single-crystal diffraction structures. As illustrated in Figure 2a, the structural unit of **PTS{1'}** is defined by two $\mathbf{PTS^{4-}}$ platforms encapsulating four guest molecules **1**. These aromatic $\mathbf{PTS^{4-}}$ platforms are organized in a "face-to-face" manner, albeit with a slight offset between the planes. The ammonium group of **1** establishes two H-bonds ($d_{N\cdots O}$ = 2.822 Å and 2.895 Å) with two unique sulfonate groups of the $\mathbf{PTS^{4-}}$, with a bridging water molecule also contributing to this H-bonding network ($d_{N\cdots O}$ = 2.722 Å). Each **PTS{1'}** unit interlinks through two types of I···O halogen-bonding interactions (3.264 Å and 3.022 Å) among adjacent molecule **1** entities (Figure S8). Upon introducing $\mathbf{A_2G^+}$ during the crystallization process of $\mathbf{PTS^{4-}}$ and **1**, we obtained **PTS{1}**. Fascinatingly, differently to our prior "Pyrene box" systems, where the $\mathbf{A_2G^+}$ cation typically co-crystallizes alongside the $\mathbf{PTS^{4-}}$ platforms,[42] **PTS{1}** crystal structure did not contain $\mathbf{A_2G^+}$ cation. We suppose that $\mathbf{A_2G^+}$ acts as a template, modifying the crystal configuration during crystallization without being an integral part of the final structure. In **PTS{1}**, there is a heightened misalignment between the two $\mathbf{PTS^{4-}}$ platforms and a diminished interplanar gap (Figure 2b). This configuration enables the ammonium group to create direct hydrogen bonds with the sulfonate groups bridging the $\mathbf{PTS^{4-}}$ platforms ($d_{N\cdots O}$ = 2.810 Å and 2.744 Å). Moreover, successive **PTS{1}** units manifest both I···O (3.177 Å) and I···I (3.735 Å) halogen-bonding interactions (Figure S9b). This leads to a denser structural assembly in **PTS{1}** than in **PTS{1'}**. When $\mathbf{G^+}$ was incorporated during the crystallization of $\mathbf{PTS^{4-}}$ and **1**, the outcome was **PTSG{1}**, reminiscent of a closed "Pyrene Box". Encapsulating a single guest molecule **1** between pair of $\mathbf{PTS^{4-}}$, and $\mathbf{G^+}$ units (Figure 2c). These $\mathbf{G^+}$ units are hydrogen bonded with sulfonate groups on respective $\mathbf{PTS^{4-}}$ platforms, tightly confining the guest molecule **1** within the supramolecular cage framework. Both $\mathbf{PTS^{4-}}$ platforms are aligned face-to-face, with an even smaller interplanar gap compared to **PTS{1}**. Calculations based on its crystal structure suggests that the cavity size between two $\mathbf{PTS^{4-}}$ planes is approximately 155.52 Å^3 (Figure S10). The ammonium group of **1** directly forms hydrogen bonds ($d_{N\cdots O}$ = 2.844 Å and 2.824 Å), or through an intermediary water molecule ($d_{N\cdots O}$ = 2.850 Å), with sulfonate groups on distinct $\mathbf{PTS^{4-}}$ platforms. Additionally, adjacent **PTSG{1}** units interconnect via the I···O (3.345 Å) halogen-bonding interactions, involving molecule **1** and the sulfonate groups of the $\mathbf{PTS^{4-}}$ platforms (Figure S11). Lastly, with the use of $\mathbf{K^+}$ counter-cations during the crystallization of $\mathbf{PTS^{4-}}$ and **1**, we observed the formation of **PTSK{1}**, a "Pyrene Box" cage with an extended cavity (582.07 Å^3, Figure S10). This is realized through the coordination between of partially hydrated $\mathbf{K^+}$ and the $\mathbf{PTS^{4-}}$ platforms (Figure 2d). The structure of **PTSK{1}** encompasses four $\mathbf{PTS^{4-}}$ platforms and an equal number of guest molecules. The dihedral angle between neighboring $\mathbf{PTS^{4-}}$ platforms is 22.59º. In a manner reminiscent of the earlier-mentioned **PTSG{1}**, the ammonium group of molecule **1** forms hydrogen bonds with the sulfonate groups on the $\mathbf{PTS^{4-}}$ platforms. This can occur directly (dN···O = 2.788 or 2.838 Å) or through a

bridging water molecule (dN···O = 2.928 Å). Additionally, contiguous **PTSK{1}** units are linked through I···I (3.572 Å) halogen-bonding interactions (Figure S12).

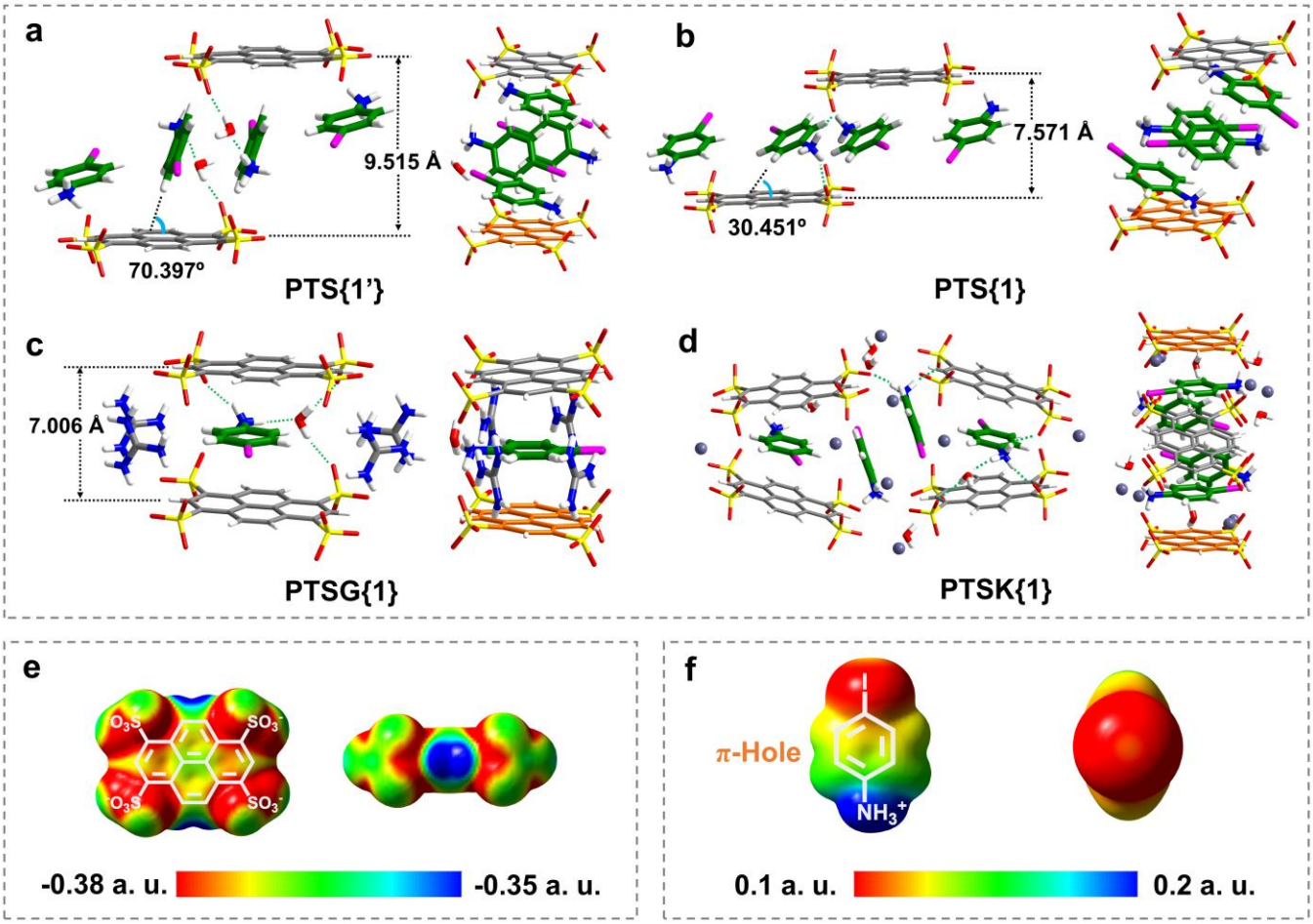

Figure 2. X-ray single crystal structures of (a) **PTS{1'}**; (b) **PTS{1}**; (c) **PTSG{1}**; (d) **PTSK{1}** and (e-f) the electrostatic potential (ESP) calculated with B3LYP/6-31+G(d, p) for main-group elements and SDD basis set for iodine atom.

To gain insight into the interactions between **PTS**$^{4-}$ and the guest molecule **1** within the crystal structure, we computed the electrostatic potential (ESP) for both **PTS**$^{4-}$ and **1**. The ESP provides a depiction of the electrostatic interaction that a positively charged test molecule would experience in the vicinity of another molecule, thereby illustrating variations in electron density distribution. As illustrated in Figure 2(e-f), areas with high electron density are marked in red, regions with standard density are yellow, and those with lower electron density are blue. For the protonated guest molecule **1**, the molecule is predominantly electron-deficient. This deficiency is accentuated by the potent electron-withdrawing capability of the -NH_3^+ group, with the maximum ESP values for the π-hole and the outer surface region of the iodine atom along the C-I covalent bond axis is being 661.17 kJ·mol^{-1} and 330.15 kJ·mol^{-1}, respectively (Figure S13-14, Table S2-5). Thus, interactions between the host and guest molecules primarily manifest as either CH-π or π-hole···π interactions, contingent on the specific cations present during crystallization. Notably, the incorporation of the sulfonate groups elevates the electrostatic potential of the **PTS**$^{4-}$, peaking at -977.72 kJ·mol^{-1} at the central region of the **PTS**$^{4-}$ platform. This elevation likely amplifies the π-hole···π interaction, especially evident in **PTSG{1}** and **PTSK{1}**.[43]

Photophysical properties. Subsequently, we delved into a thorough examination of the luminescent properties of the four cocrystal samples. As depicted in Figure S15, each of these samples showcased a broad absorption band spanning from 450 to 700 nm. Notably, **PTS{1}** manifested a pronounced absorption peak at 531 nm. Such observations can be traced back to the establishment of intermolecular charge transfer (CT) complexes in the ground state, which arise due to interactions between the electron-deficient **1** and the electron-rich **PTS**$^{4-}$ molecules present in all system.[44] The experimental observations were further supported by theoretical analyses. Specifically, the Natural Transition Orbitals (NTOs) of the four crystal structures, derived from Time-Dependent Density Functional Theory (TDDFT) calculations using the CAMB3LYP functional (Figures S16-19), show-cased the localization of holes on the π-surface of the **PTS**$^{4-}$ platforms and electrons on the molecule **1**. This distinct localization strongly suggests the existence of a charge transfer (CT) transition. Notably, the computed oscillator strength, with values ranging from 0.5139 to 0.5996, achieved a significant magnitude, affirming the detectability of the CT band in the UV-vis absorption spectra. We next undertook a comprehensive examination of the photoluminescence (PL) spectra for the four crystal samples. As depicted in Figure 3a and Figure S20, both **PTS{1'}** and **PTS{1}** showcase similar excitation patterns, accompanied by multiple emission characteristics that span from the visible to the NIR range.

For **PTS{1'}**, pronounced emission peaks appear at 489 nm, 654 nm, and 728 nm. Based on fluorescence life time, the emission peak at 489 nm, with a duration of 1.49 ns, is traced back to the fluorescence (^{1}CT) originating from the **PTS**$^{4-}$ platform. Lifetimes for the emission peaks at 654 nm and 728 nm are 4.06 ms and 4.30 ms, respectively. Furthermore, residual emission signals lasting around 20 ms are discernible between 600-800 nm, underscoring their phosphorescent nature (Figure S21-S22). Similarly,

PTS{1} shows a fluorescence emission at 481 nm (1.49 ns), along with phosphorescent emissions at 654 nm (2.29 ms) and 725 nm (2.31 ms) (Figures S23-S24). Intriguingly, a subtle emission peak at 588 nm emerges from **PTS{1}**, in contrast to **PTS{1'}**.

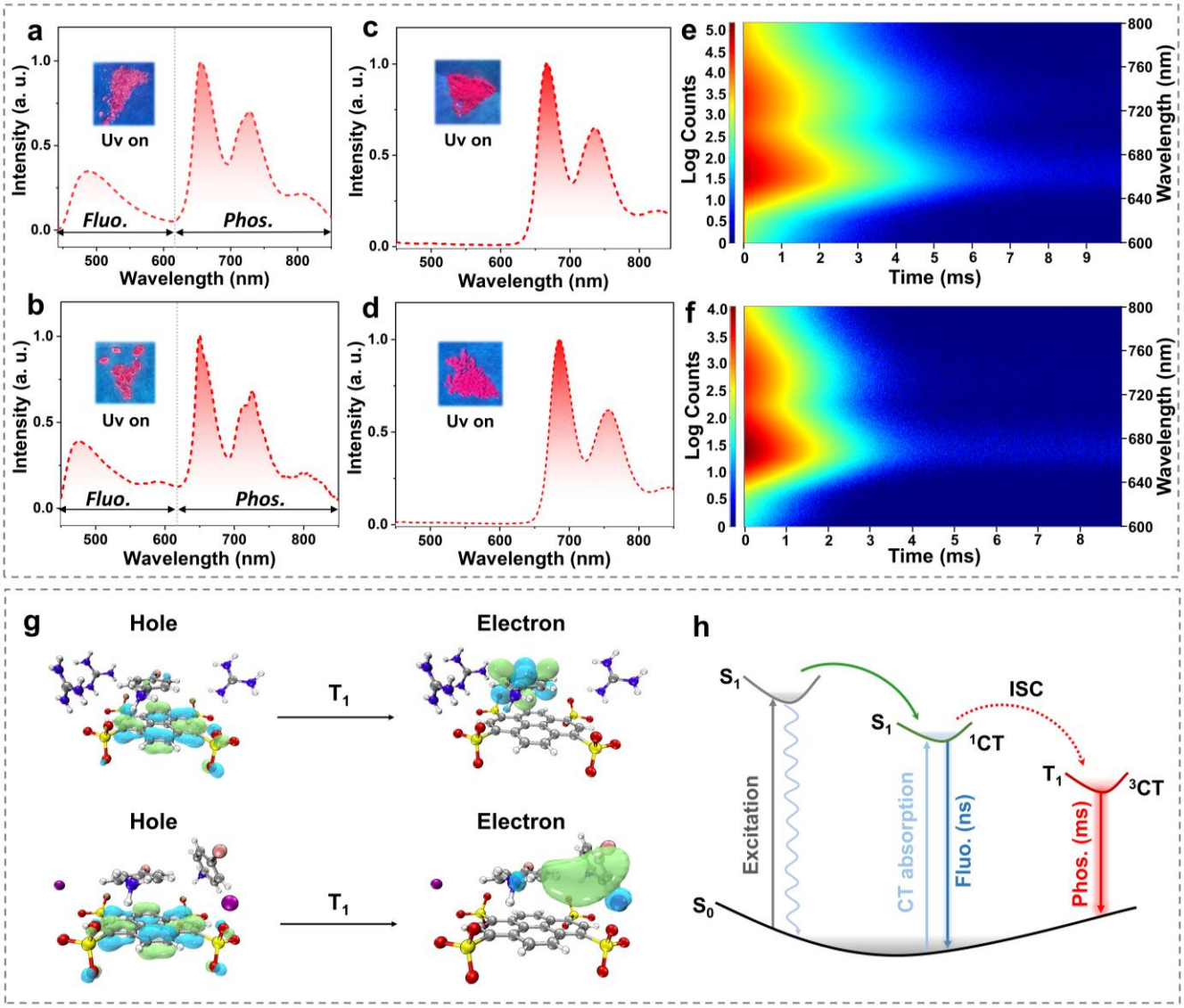

Figure 3. Room temperature photoluminescence properties of the obtained crystals upon excitation at 400 nm: (a-d) prompt emission spectra of **PTS{1'}**, **PTS{1}**, **PTSG{1}** and **PTSK{1}**; (e-f) Time resolved emission spectra of **PTSG{1}** and **PTSK{1}**; (g) Natural Transition Orbitals (NTOs) for **PTSG{1}** and **PTSK{1}** triplet states calculated at TD-CAMB3LYP level with 6-31+g(d) basis set for C, H, O and N and Lanl2dz basis set for I. The K^+ cations around chromophore molecules are replaced by unit positive charges during calculation; (h) Proposed energy transfer processes of ^{1}CT and ^{3}CT based fluorescence and phosphorescence emission.

Considering its luminescence lifetime is in the nanosecond (ns) range, combined with the enhanced intermolecular interactions between $\mathbf{PTS}^{4-}$ and **1** in **PTS{1}**, it is likely due to the emission peak from the exciplex formed between $\mathbf{PTS}^{4-}$ and **1**.[45] Lastly, the dual emission peaks around 480 nm and between 600-800 nm for both samples prompted a potential modulation of their light emission colors by adjusting the excitation wavelengths. As illustrated in Figure S25 and Table S6, **PTS{1'}** showed significant intensity variations in different emission peaks when the excitation wavelength was varied from 350 nm to 420 nm. At an excitation wavelength of 400 nm, the resultant emission displayed a CIE coordinate of (0.342, 0.321), closely mirroring white light. In a similar manner, the emission color of **PTS{1}** also underwent noticeable changes as the excitation wavelength increased, and near-white light emission (0.343,0.273) was also achieved when the excitation wavelength was at 390 nm (Figure S26, Table S7). Further examination of the excitation spectra of **PTSG{1}** and **PTSK{1}** revealed that the coordination of $\mathbf{K}^+$ ion intensifies the excitation within the 250 nm to 350 nm range (Figure S27). When excited at 400 nm, both "Pyrene Box" manifest robust emission between 600 nm and 850 nm (Figure 3c-d). Time-resolved emission spectra corroborate the phosphorescent nature of these compounds, displaying phosphorescence emission signals spanning 3-5 ms (Figure 3e-f, and Figure S28). Differently to the cocrystals **PTS{1}** and **PTS{1'}**, the use of cage templating $\mathbf{G}^+$ and $\mathbf{K}^+$ cations results in the formation of "Pyrene box" molecular cages. The confinement of guest molecule **1** amplifies the intersystem crossing (ISC) and the charge transfer process.[46] As a result, the fluorescence signal vanishes, and a red-shifted phosphorescence emission emerges relative to **PTS{1'}** and **PTS{1}**. Despite modulating the excitation wavelength, their phosphorescent emission peaks remain predominant (Figure S29). A redshift in the emission from **PTSK{1}**, relative to **PTSG{1}**, was noted. This is ascribed to a more potent coordination effect in **PTSK{1}**, where $\mathbf{K}^+$ bonds with $\mathbf{PTS}^{4-}$ more strongly than $\mathbf{G}^+$ does, increasing molecular cage rigidity and optimizing charge transfer between

the molecules. It is also noteworthy that based on the UV absorption profiles of guest molecule **1** and **PTSNa$_4$**, no significant UV absorption was detected at 400 nm for **1** (Figure S30). Consequently, the phosphorescence emission of **PTSG{1}** and **PTSK{1}** is primarily attributed to the energy absorption by **PTS^{4-}** molecules.

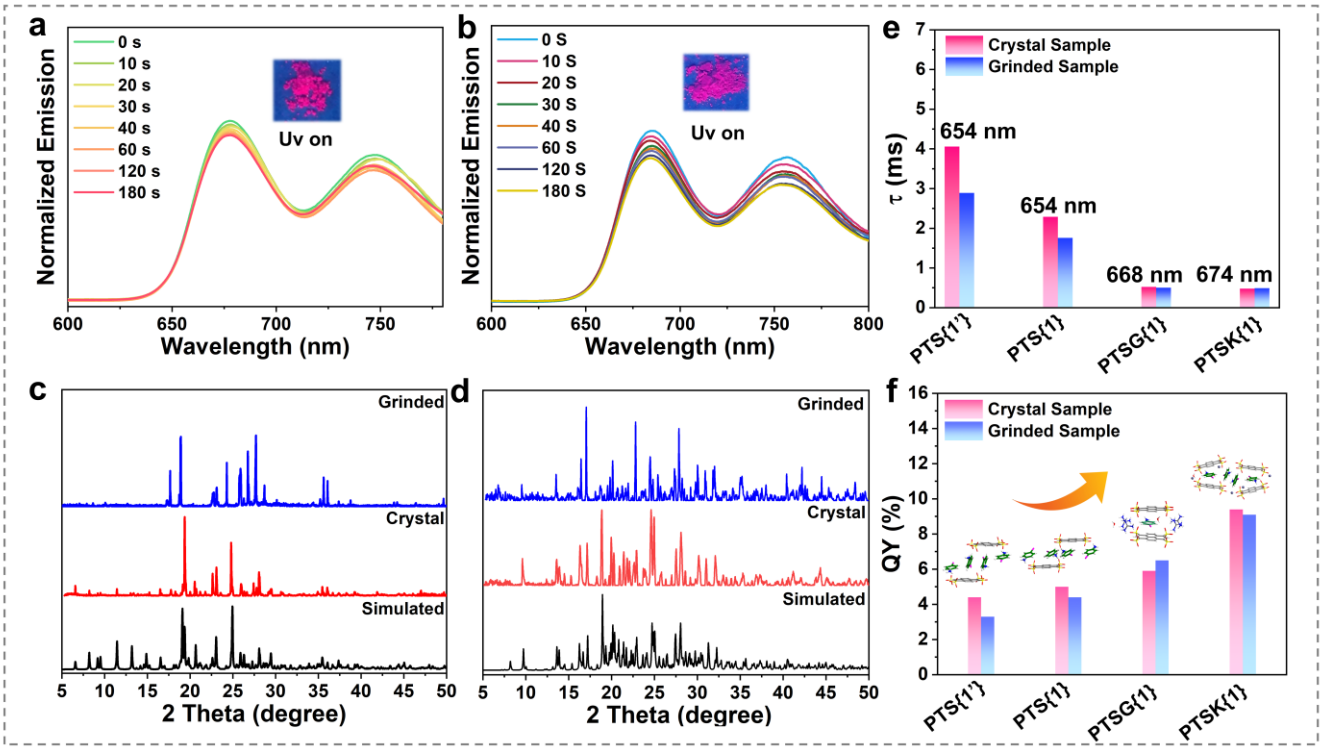

Figure 4. Steady-state PL emission spectra of (a) **PTSG{1}** and (b) **PTSK{1}** crystalline samples upon different grinding times (The inserted photos are the samples after grinding under 365 nm UV lamp); The PXRD patterns of the simulated and crystal samples as well as grinded samples of the (c) **PTSG{1}** and (d) **PTSK{1}**; (e-f) The comparison of the lifetime and quantum yield of phosphorescence emission before and after grinding.

Therefore, the possibility of fluorescence resonance energy transfer (FRET) between the host and guest molecules can be excluded. To further discern the impact of the heavy atom effect of iodine on phosphorescence emission, we synthesized **PTSK{2}**, substituting iodine with bromine. While the crystal structure of **PTSK{2}** is isostructural with **PTSK{1}** (Figure S31), pronounced residual fluorescence emission was detected. Remarkably, fluorescence emission from **PTSK{2}** exhibits a redshift compared to **PTSNa$_4$** (Figure S32). This underlines both the pivotal role of iodine's heavy atom effect in enabling phosphorescence and the ongoing charge transfer between the host and guest molecules in **PTSK{1}**.[47] The emission spectrum of **PTSNa$_4$** at 77 K reaffirms that the NIR RTP emission in the four mentioned cocrystal systems stems from the ^{3}CT of the **PTS^{4-}** platform.

Theoretical computations using the CAMB3LYP functional in TDDFT also unveiled the charge-transfer nature of the triplet state in all four samples (Figure 3g, Figures S33-36). The inclusion of counter cations introduces an excited charge transfer (^{3}CT) state (Figure 3h), leading to significant changes in orbital participation during S1 and T1 excitation, which in turn, optimizes the ISC process from S1 to T1. Further analyses estimated the phosphorescence lifetime and the rate constants for both radiative (k_r^P) and nonradiative (k_{nr}^P) transitions. This suggests that while encapsulating guest molecule **1** favor the ISC process in "Pyrene Box" systems, it also amplifies k_r^P and k_{nr}^P, resulting in a substantially reduced phosphorescence lifetime (0.48-0.53 ms) (Figure S37-S38). Room temperature measurements of the phosphorescent quantum yields of the four samples revealed an increase in quantum yield with an increasing crystalline packing density and the gusts encapsulation effect. Notably, **PTSK{1}** present a quantum yield of 9.4% (Table S8), which is highly competitive compared to other reported RTP materials in the deep-red to NIR range (Figure S39).[22-27] Earlier literature posits that the σ-hole···π interaction is vital for efficient RTP emission in cocrystal systems of pyrene and iodine-substituted aromatic derivatives, but π-hole···π interactions can quench both fluorescence and phosphorescence.[31] The data presented herein underscores our design strategy's potential, enhancing through-space charge transfer (^{3}CT) between the donor and acceptor and boosting the ISC process, resulting in an amplified RTP emission intensity and wavelength.

It's well-established that room-temperature phosphorescent materials are sensitive to oxygen and ambient conditions.[48] To gauge the influence of the "Pyrene box" molecular cage on luminescent stability, we assessed the emission spectra of all four samples across different grinding durations. Results revealed that the phosphorescent emission of **PTS{1'}** and **PTS{1}** progressively waned as grinding time increased (Figure S40). In contrast, the phosphorescent emission from the "Pyrene box" configurations remained largely unchanged throughout the same grinding periods (Figures 4a-b). Furthering our exploration, we analyzed the PXRD patterns of the samples. Evident from Figure 4c-d and Figure S41-42, the diffraction peaks for every crystal sample matched well with patterns simulated based on the crystal data. This not only verified the phase purity of these cocrystals but also emphasized that no substantial phase alterations occurred post-grinding. Wrapping up our assessment, a comparison of phosphorescence lifetimes and quantum yields, pre and post-grinding, underscored the impressive stability of the "Pyrene box" molecular cages' RTP emission characteristics (Figure 4e-f and Figure S43).

To get deeper insights into the RTP emission behaviors of the four samples, we undertook temperature-dependent emission spectrum measurements. Initially, our investigation focused on the spectral changes within the 320 K to 420 K temperature interval.

Results revealed that increasing temperatures uniformly decrease the emission intensities of all four samples, as visualized in Figure S44. This decline can primarily be attributed to heightened non-radiative transitions induced by the temperature increment. Notably, enhanced crystal packing in Pyrene boxes density fortified the resilience of phosphorescent emission against temperature fluctuations.

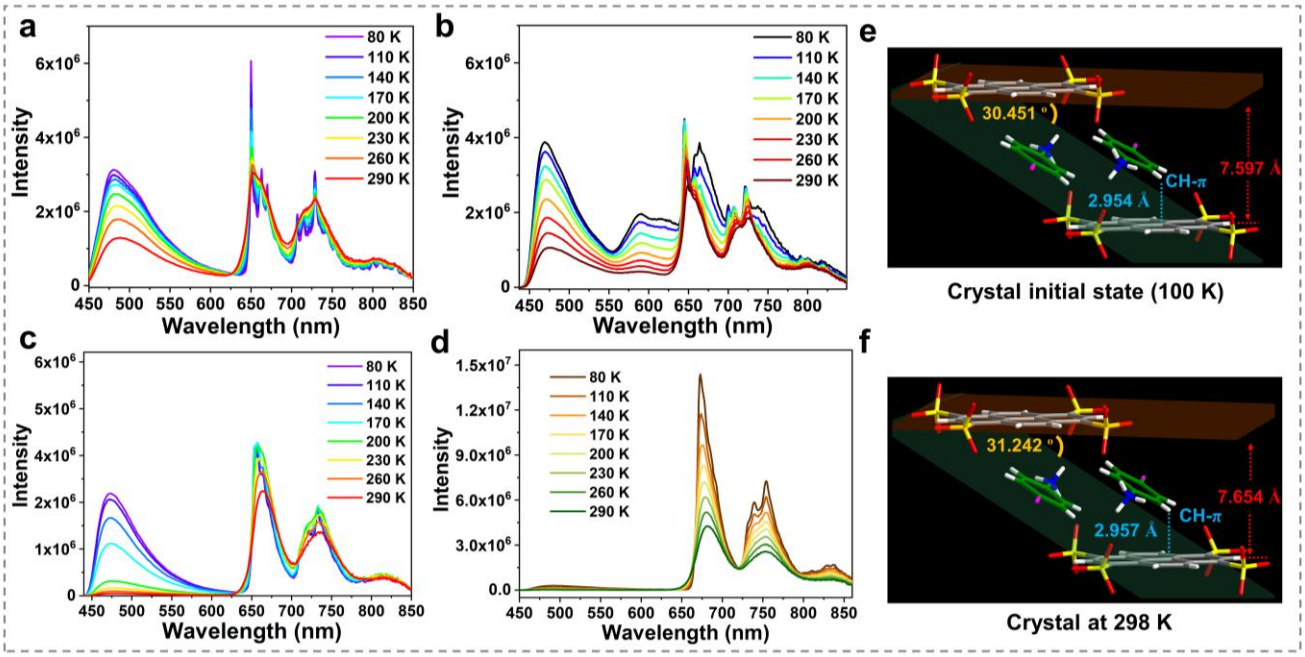

Figure 5. Temperature-dependent emission spectra of the crystalline samples: (a) **PTS{1'}**; (b) **PTS{1}**; (c) **PTSG{1}**; (d) **PTSK{1}** upon the excitation at 400 nm. (e) and (f) are the crystal structure of **PTS{1}** at RT or 100 K.

Specifically, "Pyrene box" cage superstructures **PTSG{1}** and **PTSK{1}**, maintained robust phosphorescent emissions even at the elevated temperature of 420 K. TGA analysis showed their decomposition above 200 ºC (Figure S45). Contrastingly, the cryogenic emission spectra of the four crystalline structures showcased diverse reactions to temperature variations, a result of their unique structural configurations. Lowering the temperature from 290 K down to 80 K, the fluorescence intensity of **PTS{1'}**, surged while its phosphorescent emission underwent modest augmentation, accompanied by the emergence of a vibrational split in the emission peak (Figure 5a). The fluorescence and phosphorescence lifetimes similarly expanded in tandem with temperature reduction, mirroring the fluorescence intensity's trajectory (Figure S46). For **PTS{1}**, as the temperature dropped, the fluorescence emissions at 481 nm and 588 nm, in concertation with the phosphorescence emission and their respective lifetimes, showed incremental increased values (Figure 5b and Figure S47). Intriguingly, the phosphorescence emission peak of **PTS{1}** bifurcated and manifested a subtle red-shift during this temperature descent. A comparative examination of **PTS{1}**'s crystal structure at room temperature and 80 K show that at low temperature inter planar distances between $\mathbf{PTS^{4-}}$ platforms are reduced together with the halogen bonding lengths (C-I···I-C) within $\mathbf{PTS^{4-}}$ units (Figure 5e-f and Figure S9). Concurrently, the dihedral angle between the guest molecule **1** and the $\mathbf{PTS^{4-}}$ platform decrease. This led us to postulate that the observed spectral bifurcation and redshift in **PTS{1}** is related from the diminished spatial relationship and angle between the guest molecule **1** and the $\mathbf{PTS^{4-}}$ platform, increasing the electrostatic interplay between the Donnor ($\mathbf{PTS^{4-}}$) and Acceptor (**1**) units.[49] This is confirmed by the properties of the "Pyrene Box" molecular cage **PTSG{1}**, when both fluorescence and phosphorescence intensities and their lifetimes exhibited marked improvements with declining temperatures (Figure 5c and Figure S48). Notably, fluorescence emission showed a significant increase below the 200 K, underlining a pronounced role of singlet non-radiative transitions in energy dispersion. In contrast, **PTSK{1}** maintained a minimal residual fluorescence peak during cooling. Instead, its phosphorescent emission and associated lifetime notably increased with decreasing temperatures (Figure 5d and Figure S49), which indicates an efficient intersystem crossing process in **PTSK{1}**.

pH-response behavior. Considering the presence of protonated amino groups in the crystalline systems, which suggests potential pH-responsive behavior,[50, 51] we followed our investigation to test their efficacy in the fluorescence sensing of organic amine gases. Triethylamine (TEA), known for its high volatility, was chosen as the representative compound for our study. Notably, the phosphorescence emission of **PTS{1'}** and **PTS{1}** crystal samples was swiftly quenched upon the dropwise addition of a small volume of TEA (Figure S50, Supplementary Movie 1-2). Moreover, when these quenched samples were subsequently exposed to hydrochloric acid vapor, their phosphorescence emission was revived within hours. We infer from these observations that the sensing mechanism might entail the deprotonation of guest molecules in the co-crystal by the alkaline TEA gas and lead to a progressive partial loss of the crystallinity. This process disrupts the ^{3}CT transition, leading to the attenuation of phosphorescence emission. Interestingly, the "Pyrene box" systems, specifically **PTSG{1}** and **PTSK{1}**, demonstrated distinct fluorescence reactions to basic TEA gas (Figure 6a). For **PTSG{1}**, its phosphorescence emission remained unaltered in the presence of TEA gas (Supplementary Movie 3). We surmise that this stability stems from the formation of compact "Pyrene Box" cages via strong hydrogen bonding between $\mathbf{G^+}$ and the $\mathbf{PTS^{4-}}$, which protect the guest molecules from ready deprotonation. Differently, **PTSK{1}** showed a swift emission color alteration upon exposure to TEA gas, shifting from red to a luminous green in under a second (Supplementary Movie 4). Further PL analysis revealed a consistent decline in phosphorescence emission in the 650 nm to 850 nm range over time, while showing a surge in $\mathbf{PTS^{4-}}$ green fluorescence emission around 500 nm with a quantum yield of 18% (Figure 6b-c, Table S9).

To gain a deeper understanding of the fluorescence sensing mechanism, we measured the solid-state UV absorption spectra of the four crystal samples after TEA fumigation. The results showed that the absorption range of all the samples beyond 500 nm has broadened (Figure S51). Particularly, the CT absorption peak of **PTS{1}** around 550 nm has significantly decreased after exposure to TEA vapor, confirming that the TEA fumigation alters the charge transfer transition characteristics between the host and guest molecules, thereby changing the phosphorescence properties of the **PTS**$^{4-}$.

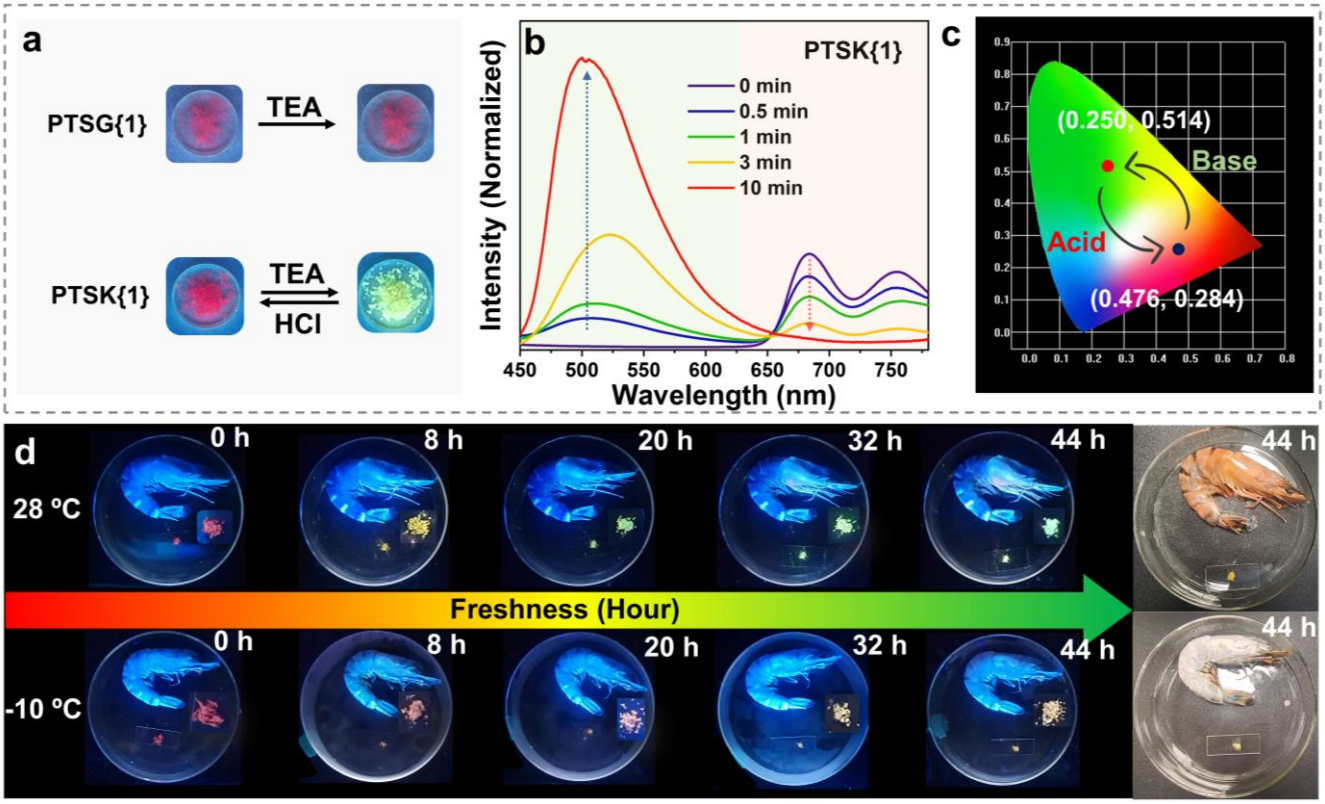

Figure 6. Amine-response behavior of the "Pyrene box" systems. (a) The photos demonstrating the responsiveness of **PTSG{1}** and **PTSK{1}** to TEA. (b) The emission spectra of **PTSK{1}** at different time intervals upon interaction with TEA and (c) The CIE coordinates. (d) Images showcasing the use of **PTSK{1}** with an initial red phosphorescence as a smart trademark for monitoring the freshness of shrimps stored under various conditions.

We subsequently analyzed the infrared spectra of the four samples both pre- and post-exposure to TEA vapors. For **PTS{1'}** and **PTS{1}**, -NH_3^+ absorption peaks were evident around 3000 cm^{-1} and 2600 cm^{-1} (Figure S52).[52] In vapor-exposed samples, the intensity of these signals diminished, but sharp -NH_2 absorption peaks emerged around 3300 cm^{-1}, reminiscent with the deprotonation of the guest molecules. Remarkably, the IR spectrum of **PTSG{1}** remained largely consistent before and after TEA vapor exposure (Figure S53a), attesting to its exceptional resilience against TEA. Meanwhile, for **PTSK{1}**, a diminished -NH_3^+ absorption peak was discerned around 2600 cm^{-1} post-exposure, along with a faint -NH_2 peak at approximately 3400 cm^{-1} (Figure S53b). Given that the deep-red phosphorescence of restored crystalline **PTSK{1}** could be rejuvenated after several hours of exposure to HCl vapor, we equate that deprotonation of guest molecules is the driving force of the phosphorescence/fluorescence transition in **PTSK{1}**. Contrary to the cocrystal systems of **PTS{1'}** and **PTS{1}**, the coordination of K^+ ions stabilizes the position of the **PTS**$^{4-}$ platforms, and the guest molecule's insertion mitigates the aggregation caused quenching (ACQ) effect of **PTS**$^{4-}$. This leads to the energy dissipation through its ^{1}CT radiative transition channel upon TEA interaction. Finally, we further investigated the cyclic nature of **PTSK{1}**'s response to TEA and HCl stimulation. The pH responsiveness was limited to a single complete cycle. Upon a second exposure to HCl on the TEA-treated **PTSK{1}** sample, only a partial restoration of its phosphorescence was observed (Figure S54). Notably, **PTSK{1}**, in addition to its remarkable sensitivity to TEA, displayed commendable fluorescence detection capabilities for NH_3 gas (Supplementary Movie 5). We know organic amines are critical derivatives of biogenic amines released during amino acid sea food degradation, positioning **PTSK{1}** as a potential ratiometric fluorescence probe for seafood freshness.[53] Subsequently, we evaluated the applicability of **PTSK{1}** for assessing the freshness of shrimp using fluorescence detection. As illustrated in Figure 6d, fresh shrimp were co-encapsulated with a small quantity of **PTSK{1}** crystal samples in the same airtight container. These were then stored at room temperature (28 °C) and at a low temperature of -10 °C for 44 hours, respectively. At various time points, we photographed the luminescence color of the **PTSK{1}** samples under ultraviolet light. Notably, biogenic amines released as the shrimp deteriorated at room temperature, instigated a shift in **PTSK{1}** emission from red to yellow, and then in green. Conversely, in the frozen state, this transition markedly decelerated, with the sample primarily showcasing a yellow hue even after 44 hours. To discount the potential impact of water vapor on the luminescence color variation of **PTSK{1}**, it was co-located with a minuscule amount of aqueous solution in a sealed chamber. A post-15-hour examination revealed an unchanged luminescence color, affirming **PTSK{1}**'s luminance color stability in moist settings (Figure S55). These insights conclusively establish **PTSK{1}**'s prowess in real-time, naked-eye detection of gaseous biogenic amines, underscoring its prospective utility as a smart indicator for seafood freshness monitoring.

CONCLUSION

In summary, we successfully synthesized an impressive range of structurally diverse deep-red to NIR RTP cocrystal materials. This achievement was made possible through meticulous control of the crystallization process between Donnor host ($\mathbf{PTS^{4-}}$) and Acceptor guest (**1**) units by introducing various cationic entities ($\mathbf{A_2G^+}$, $\mathbf{G^+}$, or $\mathbf{K^+}$) in the formation of "Pyrene box". We observed a sequential shift in the excited states of the cocrystal from a mixed singlet-triplet state to a predominantly triplet state, accompanied by an increase in phosphorescence quantum yield. Both experimental results and TDDFT computational studies revealed that the encapsulation effect of the self-assembled "Pyrene box" molecular cages significantly enhanced charge transfer between the host and guest molecules. This mechanism also suppressed molecular vibrations, expedited the intersystem crossing (ISC) process, and led to intensified bathochromic phosphorescent emissions. Intriguingly, due to the environmental sensitivity of the phosphorescent emission, these materials demonstrated a strong fluorescence pH-response to fuming gases such as triethylamine or ammonia. This suggests potential applications in early detection of shrimp or sea-food spoilage. Our research not only introduces an innovative design strategy and environmentally friendly synthesis for deep-red to NIR RTP materials, but also paves the way for expanding gas sensing applications in the field of organic RTP materials.

ASSOCIATED CONTENT

Supporting Information. Supplementary NMR, X-ray diffraction, additional experimental synthesis, photophysical, thermal properties, computational data, and other experimental details are available free of charge via the Internet at http://pubs.acs.org.

AUTHOR INFORMATION

Corresponding Author

*E-mail: mihail-dumitru.barboiu@umontpellier.fr;
fwxdk@nwpu.edu.cn;
hongxiayan@nwpu.edu.cn.

Author Contributions

The manuscript was written through contributions of all authors which have given approval to the final version of the manuscript.

ACKNOWLEDGMENT

This work is funded by the National Natural Science Foundation of China (22001212, 22175143). The authors also would like to thank the Analytical & Testing Center of Northwestern Polytechnical University for TGA and PXRD testing.

REFERENCES

(1) Wang, T.; Su, X.; Zhang, X.; Nie, X.; Huang, L.; Zhang, X.; Sun, X.; Luo, Y.; Zhang, G., Aggregation- induced dual- phosphorescence from organic molecules for nondoped light- emitting diodes. *Adv. Mater.* **2019**, *31* (51), 1904273.

(2) Su, Y.; Phua, S. Z. F.; Li, Y.; Zhou, X.; Jana, D.; Liu, G.; Lim, W. Q.; Ong, W. K.; Yang, C.; Zhao, Y., Ultralong room temperature phosphorescence from amorphous organic materials toward confidential information encryption and decryption. *Sci. adv.* **2018**, *4* (5), eaas9732.

(3) Fu, P. Y.; Li, B. N.; Zhang, Q. S.; Mo, J. T.; Wang, S. C.; Pan, M.; Su, C. Y., Thermally activated fluorescence vs long persistent luminescence in ESIPT-attributed coordination polymer. *J. Am. Chem. Soc.* **2022**, *144* (6), 2726-2734.

(4) Ye, W.; Ma, H.; Shi, H.; Wang, H.; Lv, A.; Bian, L.; Zhang, M.; Ma, C.; Ling, K.; Gu, M.; Mao, Y.; Yao, X.; Gao, C.; Shen, K.; Jia, W.; Zhi, J.; Cai, S.; Song, Z.; Li, J.; Zhang, Y.; Lu, S.; Liu, K.; Dong, C.; Wang, Q.; Zhou, Y.; Yao, W.; Zhang, Y.; Zhang, H.; Zhang, Z.; Hang, X.; An, Z.; Liu, X.; Huang, W., Confining isolated chromophores for highly efficient blue phosphorescence. *Nat Mater* **2021,** *20* (11), 1539-1544.

(5) Dai, W.; Niu, X.; Wu, X.; Ren, Y.; Zhang, Y.; Li, G.; Su, H.; Lei, Y.; Xiao, J.; Shi, J., Halogen bonding: a new platform for achieving multi- stimuli- responsive persistent phosphorescence. *Angew. Chem.* **2022**, *134* (13), e202200236.

(6) Zhang, Y.; Chen, X.; Xu, J.; Zhang, Q.; Gao, L.; Wang, Z.; Qu, L.; Wang, K.; Li, Y.; Cai, Z., Cross-linked polyphosphazene nanospheres boosting long-lived organic room-temperature phosphorescence. *J. Am. Chem. Soc.* **2022**, *144* (13), 6107-6117.

(7) Wang, X. F.; Xiao, H.; Chen, P.-Z.; Yang, Q. Z.; Chen, B.; Tung, C. H.; Chen, Y. Z.; Wu, L. Z., Pure organic room temperature phosphorescence from excited dimers in self-assembled nanoparticles under visible and near-infrared irradiation in water. *J. Am. Chem. Soc*. **2019**, *141* (12), 5045-5050.

(8) Jin, J.; Jiang, H.; Yang, Q.; Tang, L.; Tao, Y.; Li, Y.; Chen, R.; Zheng, C.; Fan, Q.; Zhang, K. Y.; Zhao, Q.; Huang, W., Thermally activated triplet exciton release for highly efficient tri-mode organic afterglow. *Nat. Commun.* **2020**, *11* (1), 842.

(9) Ma, X.-K.; Liu, Y., Supramolecular purely organic room-temperature phosphorescence. *Acc. Chem. Res.* **2021**, *54* (17), 3403-3414.

(10) Yang, J.; Zhen, X.; Wang, B.; Gao, X.; Ren, Z.; Wang, J.; Xie, Y.; Li, J.; Peng, Q.; Pu, K.; Li, Z., The influence of the molecular packing on the room temperature phosphorescence of purely organic luminogens. *Nat. Commun.* **2018**, *9* (1), 840.

(11) Roy, B.; Maisuls, I.; Zhang, J.; Niemeyer, F. C.; Rizzo, F.; Wölper, C.; Daniliuc, C. G.; Tang, B. Z.; Strassert, C. A.; Voskuhl, J., Mapping the regioisomeric space and visible color range of purely organic dual emitters with ultralong phosphorescence components: from violet to red towards pure white light. *Angew. Chem. Int. Ed.* **2022**, *61* (4), e202111805.

(12) Song, J.; Zhou, Y.; Pan, Z.; Hu, Y.; He, Z.; Tian, H.; Ma, X., An elastic organic crystal with multilevel stimuli-responsive room temperature phosphorescence. *Matter*, **2023**, *6*, 1-14.

(13) Zhang, X.; Du, L.; Zhao, W.; Zhao, Z.; Xiong, Y.; He, X.; Gao, P. F.; Alam, P.; Wang, C.; Li, Z.; Leng, J.; Liu, J.; Zhou, C.; Lam, J. W. Y.; Phillips, D. L.; Zhang, G.; Tang, B. Z., Ultralong uv/mechano-excited room temperature phosphorescence from purely organic cluster excitons. *Nat Commun* **2019,** *10* (1), 5161.

(14) Wei, P.; Zhang, X.; Liu, J.; Shan, G. G.; Zhang, H.; Qi, J.; Zhao, W.; Sung, H. H.; Williams, I. D.; Lam, J. W. Y.; Tang, B. Z., New wine in old bottles: prolonging room-temperature phosphorescence of crown ethers by supramolecular interactions. *Angew. Chem. Int. Ed*. **2020**, *59* (24), 9293-9298.

(15) Singh, M.; Liu, K.; Qu, S.; Ma, H.; Shi, H.; An, Z.; Huang, W., Recent advances of cocrystals with room temperature phosphorescence. *Adv. Opt. Mater*. **2021**, *9* (10), 2002197.

(16) Sun, L.; Wang, Y.; Yang, F.; Zhang, X.; Hu, W., Cocrystal engineering: a collaborative strategy toward functional materials. *Adv. Mater*. **2019**, *31* (39), e1902328.

(17) Zhuo, M. P.; Yuan, Y.; Su, Y.; Chen, S.; Chen, Y. T.; Feng, Z. Q.; Qu, Y. K.; Li, M. D.; Li, Y.; Hu, B. W.; Wang, X. D.; Liao, L. S., Segregated array tailoring charge-transfer degree of organic cocrystal for the efficient near-infrared emission beyond 760 nm. *Adv. Mater*. **2022**, *34* (11), e2107169.

(18) Wang, Y.; Wu, H.; Li, P.; Chen, S.; Jones, L. O.; Mosquera, M. A.; Zhang, L.; Cai, K.; Chen, H.; Chen, X. Y.; Stern, C. L.; Wasielewski, M. R.; Ratner, M. A.; Schatz, G. C.; Stoddart, J. F., Two-photon excited deep-red and near-infrared emissive organic co-crystals. *Nat Commun*, **2020**, *11* (1), 4633.

(19) Sun, L.; Zhu, W.; Zhang, X.; Li, L.; Dong, H.; Hu, W., Creating organic functional materials beyond chemical bond synthe-

sis by organic cocrystal engineering. *J. Am. Chem. Soc*. **2021**, *143* (46), 19243-19256.
(20) Zhao, W.; He, Z.; Tang, B. Z., Room-temperature phosphorescence from organic aggregates. *Nat. Rev. Mater*., **2020**, *5* (12), 869-885.
(21) Huang, Y.; Wang, Z.; Chen, Z.; Zhang, Q., Organic cocrystals: beyond electrical conductivities and field-effect transistors (FETs). *Angew. Chem. Int. Ed*. **2019**, *58*, 9696-9711.
(22) Zhu, T.; Yang, T.; Zhang, Q.; Yuan, W. Z., Clustering and halogen effects enabled red/near-infrared room temperature phosphorescence from aliphatic cyclic imides. *Nat. Commun.* **2022**, *13* (1), 2658.
(23) Ono, T.; Kimura, K.; Ihara, M.; Yamanaka, Y.; Sasaki, M.; Mori, H.; Hisaeda, Y., Room-temperature phosphorescence emitters exhibiting red to near-infrared emission derived from intermolecular charge-transfer triplet states of naphthalenediimide-halobenzoate triad molecules. *Chem. Eur. J*. **2021**, *27* (37), 9535-9541.
(24) Wang, Z.; Liu, J. J.; Yin, S. Y.; Li, M. Y.; Hou, Y. J.; Wang, D.; Mo, J. T.; Chen, G., Ultralong near infrared room temperature phosphorescence in Cu (I) metal- organic framework based- on D–π–A–π–D linkers. *Adv. Funct. Mater.* **2023**, *33* (16), 2212985.
(25) Wu, H.; Wang, D.; Zhao, Z.; Wang, D.; Xiong, Y.; Tang, B. Z., Tailoring noncovalent interactions to activate persistent room- temperature phosphorescence from doped polyacrylonitrile films. *Adv. Funct. Mater.* **2021**, *31* (32), 2101656.
(26) Wang, Z.; Li, A.; Zhao, Z.; Zhu, T.; Zhang, Q.; Zhang, Y.; Tan, Y.; Yuan, W. Z., Accessing excitation- and time- responsive afterglows from aqueous processable amorphous polymer films through doping and energy transfer. *Adv. Mater.* **2022**, *34* (31), 2202182.
(27) Xiao, F.; Gao, H.; Lei, Y.; Dai, W.; Liu, M.; Zheng, X.; Cai, Z.; Huang, X.; Wu, H.; Ding, D., Guest-host doped strategy for constructing ultralong-lifetime near-infrared organic phosphorescence materials for bioimaging. *Nat. Commun.* **2022**, *13* (1), 186.
(28) Feng, C.; Li, S.; Xiao, X.; Lei, Y.; Geng, H.; Liao, Y.; Liao, Q.; Yao, J.; Wu, Y.; Fu, H., Excited-state modulation for controlling fluorescence and phosphorescence pathways toward white‐light emission. *Adv. Opt. Mater*. **2019**, *7* (20), 1900767.
(29) Wang, W.; Zhang, Y.; Jin, W. J., Halogen bonding in room-temperature phosphorescent materials. *Coord. Chem. Rev*. **2020**, *404*, 213107.
(30) Ding, X. H.; Chang, Y. Z.; Ou, C. J.; Lin, J. Y.; Xie, L. H.; Huang, W., Halogen bonding in the co-crystallization of potentially ditopic diiodotetrafluorobenzene: a powerful tool for constructing multicomponent supramolecular assemblies. *Nat. Sci. Rev*. **2020**, *7* (12), 1906-1932.
(31) Abe, A.; Goushi, K.; Mamada, M.; Adachi, C., Organic binary and ternary cocrystal engineering based on halogen bonding aimed at room- temperature phosphorescence. *Adv. Mater.* **2023**, 2211160.
(32) Gao, R.; Cha, Y.; Ahmad, H. M.; Fu, H.; Yu, Z., Loose cocrystal strategy for high-efficiency near-infrared phosphorescence. *Adv. Opt. Mater*., **2023**, 2301112.
(33) Avinash, M. B.; Govindaraju, T., Architectonics: Design of molecular architecture for functional applications. *Acc. Chem. Res*. **2018**, *51*(2), 414-426.
(34) Dumitrescu, D.; Legrand, Y. M.; Petit, E.; van Der Lee, A.; Barboiu, M., Progressive compression of 1, ω-diammonium-alkanes inside a rigid crystalline molecular cage. *Chem. Commun.* **2014,** *50* (91), 14086-14088.
(35) Feng, W. X.; Van Der Lee, A.; Legrand, Y. M.; Petit, E.; Su, C. Y.; Barboiu, M., "Pyrene Box" cages for the confinement of biogenic amines. *Chem. Eur. J.* **2017,** *23* (17), 4037-4041.
(36) Dumitrescu, D.; Dumitru, F.; Legrand, Y. M.; Petit, E.; van Der Lee, A.; Barboiu, M., New "Pyrene Box" cages for adaptive guest conformations. *Org. Lett.* **2015,** *17* (9), 2178-2181.
(37) Feng, W. X.; van Der Lee, A.; Legrand, Y.-M.; Petit, E.; Dumitrescu, D.; Su, C. Y.; Barboiu, M., Adaptive encapsulation of ω-Amino acids and their guanidinium-amide congeners. *Org. Lett.* **2016,** *18* (21), 5556-5559.
(38) Feng, S.; Huang, Q.; Yang, S.; Lin, Z.; Ling, Q., A metal-free 2D layered organic ammonium halide framework realizing full-color persistent room-temperature phosphorescence. *Chem. Sci.* **2021,** *12* (43), 14451-14458.
(39) Garain, S.; Ansari, S. N.; Kongasseri, A. A.; Garain, B. C.; Pati, S. K.; George, S. J., Room temperature charge-transfer phosphorescence from organic donor-acceptor Co-crystals. *Chem. Sci.* **2022,** *13* (34), 10011-10019.
(40) Garain, S.; Wagalgave, S. M.; Kongasseri, A. A.; Garain, B. C.; Ansari, S. N.; Sardar, G.; Kabra, D.; Pati, S. K.; George, S. J., Anion-π-induced room temperature phosphorescence from emissive charge-transfer states. *J. Am. Chem. Soc.* **2022,** *144* (24), 10854-10861.
(41) Partanen, I.; Al-Saedy, O.; Eskelinen, T.; Karttunen, A. J.; Saarinen, J. J.; Mrózek, O.; Steffen, A.; Belyaev, A.; Chou, P.-T.; Koshevoy, I. O., Fast and tunable phosphorescence from organic ionic crystals. *Angew. Chem.* **2023**, e202305108.
(42) Dumitrescu, D. G.; Feng, W. X.; Legrand, Y.-M.; van Der Lee, A.; Petit, E.; Barboiu, M., Pyrene-box capsules for adaptive encapsulation and structure determination of unstable or non-crystalline guest molecules. *CrystEngComm.* **2018,** *20* (3), 261-270.
(43) Li, L.; Wang, H.; Wang, W.; Jin, W. J., Interactions between haloperfluorobenzenes and fluoranthene in luminescent cocrystals from π-hole···π to σ-hole···π bonds. *CrystEngComm* **2017,** *19* (34), 5058-5067.
(44) Guo, J.; Zhen, Y.; Dong, H.; Hu, W., Recent progress on organic exciplex materials with different donor–acceptor contacting modes for luminescent applications. *J. Mater. Chem. C* **2021**, *9* (47), 16843-16858.
(45) McManus, G. J.; Perry IV, J. J.; Perry, M.; Wagner, B. D.; Zaworotko, M. J., Exciplex fluorescence as a diagnostic probe of structure in coordination polymers of Zn^{2+} and 4, 4'-bipyridine containing intercalated pyrene and enclathrated aromatic solvent guests. *J. Am. Chem. Soc.* **2007,** *129* (29), 9094-9101.
(46) Zhou, H. Y.; Zhang, D. W.; Li, M.; Chen, C. F., A Calix[3] acridan- based host-guest cocrystal exhibiting efficient thermally activated delayed fluorescence. *Angew. Chem.* **2022,** *134* (15), e202117872.
(47) Sun, M. J.; Anhalt, O.; Sarosi, M. B.; Stolte, M.; Wurthner, F., Activating organic phosphorescence via heavy metal-π interaction induced intersystem crossing. *Adv. Mater*. **2022**, *34* (51), e2207331.
(48) Song, J.; Ma, L.; Sun, S.; Tian, H.; Ma, X., Reversible multilevel stimuli-responsiveness and multicolor room-temperature phosphorescence emission based on a single-component system. *Angew. Chem. Int. Ed.* **2022,** *61* (29), e202206157.
(49) Fang, J.; Li, P.; Xue, X.; Li, H.; Cui, D.; Zhang, J.; Wang, Y.; Debnath, T.; Jie, Y.; Huang, W.; Chen, R., Realignment of local and charge-transfer excited states in promoting room-temperature phosphorescence of organic aggregates. *Chem. Mater*. **2023**. *35*, 6405-6414.
(50) Li, S.; Yan, D., Two-component aggregation-induced emission materials: Tunable one/two-photon luminescence and stimuli-responsive switches by co-crystal formation. *Adv. Opt. Mater.* **2018,** *6*, 1800445.
(51) Cheng, Z.; Shi, H.; Ma, H.; Bian, L.; Wu, Q.; Gu, L.; Cai, S.; Wang, X.; Xiong, W. w.; An, Z., Ultralong phosphorescence from organic ionic crystals under ambient conditions. *Angew. Chem. Int.*

Ed. **2018,** *57* (3), 678-682.
(52) Zhang, Q.; Wang, R.; Feng, B.; Zhong, X.; Ostrikov, K., Photoluminescence mechanism of carbon dots: triggering high-color-purity red fluorescence emission through edge amino protonation. *Nat. Commun.* **2021,** *12* (1), 6856.
(53) Jia, R.; Tian, W.; Bai, H.; Zhang, J.; Wang, S.; Zhang, J., Amine-responsive cellulose-based ratiometric fluorescent materials for real-time and visual detection of shrimp and crab freshness. *Nat. Commun.* **2019,** *10* (1), 795.

TOC Graphic